buildings

MDPI

Article

Preparation and Electromagnetic-Wave-Absorption Properties of Cement-Based Materials with Graphite Tailings and Steel Fiber

Qian Wang [1], Taibing Wei [1], Rong Wang [1], Deliang Zhu [1], Feiyu Liu [1] and Huawei Li [1,2,*]

[1] School of Civil Engineering and Architecture, Wuyi University, Wuyishan 354300, China; wangqian@wuyiu.edu.cn (Q.W.); tbwei@wuyiu.edu.cn (T.W.); wangrong@wuyiu.edu.cn (R.W.); zdl337275100@wuyiu.edu.cn (D.Z.); liufeiyu@wuyiu.edu.cn (F.L.)
[2] School of Civil and Transportation Engineering, Guangdong University of Technology, Guangzhou 510006, China
* Correspondence: hwli3880@wuyiu.edu.cn

Abstract: The development of functional building materials that can absorb electromagnetic radiation is important for preventing and controlling electromagnetic pollution in urban areas. In this study, cement-based electromagnetic wave (EMW)-absorbing materials were created using graphite tailings (GTs) as a conductive admixture and steel fiber (SF) as an EMW absorber, which resulted in materials with a wide effective bandwidth and high reflection loss (RL). In particular, a GT–cement matrix with excellent mechanical and electrical properties was obtained. This study explored the influence mechanism of the SF content on the mechanical, electrical, and EMW-absorption properties of cement-based materials under the synergistic effect of GTs and SF. Findings demonstrate that the combination of GTs and SF notably improved the electrical and EMW-absorption characteristics of the cement-based materials. Optimal EMW-absorption properties were observed for a combination of 30% GTs and 6% SF. A developed cement-based EMW-absorbing material with a thickness of 20 mm displayed a minimum RL of −25.78 dB in the frequency range of 0.1–5 GHz, with an effective bandwidth of 0.953 GHz. Thus, the cement-based composite materials developed in this study have excellent EMW-absorption performance, which provides an effective strategy for preventing and controlling electromagnetic pollution in urban spaces.

Keywords: GTs; SF; EMW-absorbing materials; electrical properties; impedance matching; RL

check for updates

Citation: Wang, Q.; Wei, T.; Wang, R.; Zhu, D.; Liu, F.; Li, H. Preparation and Electromagnetic-Wave-Absorption Properties of Cement-Based Materials with Graphite Tailings and Steel Fiber. *Buildings* **2024**, *14*, 3685. https://doi.org/10.3390/buildings14113685

Academic Editor: Yun Gao

Received: 23 October 2024
Revised: 9 November 2024
Accepted: 16 November 2024
Published: 19 November 2024

Copyright: © 2024 by the authors. Licensee MDPI, Basel, Switzerland. This article is an open access article distributed under the terms and conditions of the Creative Commons Attribution (CC BY) license (https://creativecommons.org/licenses/by/4.0/).

1. Introduction

The rapid development of the 5G network and electronic technologies has significantly improved people's daily life convenience through wireless communication equipment and electronic products [1–3]. However, it has also introduced substantial electromagnetic pollution. Electromagnetic pollution can easily lead to problems, such as electronic equipment failure and information leakage, and negatively affect people's health [4,5]. Therefore, preventing and controlling electromagnetic pollution has become a concern that needs to be addressed. The research and development of electromagnetic wave (EMW)-absorbing materials can be an effective method to alleviate electromagnetic pollution [6–8], and the EMW bands corresponding to the common used communication devices are displayed in Table 1. Cement-based materials are widely used building materials in construction engineering and can be utilized as high-quality carriers for EMW-absorbing materials. However, the EMW-absorption performance of ordinary cement-based materials is poor [9]. Using conductive fillers or absorbers is an effective way to improve the loss attenuation ability of cement-based materials for EMWs [10,11]. Therefore, a good combination of materials with strong electromagnetic loss attenuation ability and cement-based materials is crucial for preventing and controlling electromagnetic pollution in urban spaces.

Table 1. The frequency of the common used communication devices.

Frequency Range/MHz	Pollution Sources
76–108	FM Broadcasting
1880–1900 and 2010–2025	3G communication
1880–1900, 2320–2370 and 2575–2635	4G communication
3300–3400, 3400–3600 and 4800–5000	5G communication

Mine tailings are solid wastes produced in the process of mining mineral resources, and their utilization can effectively reduce environmental pollution [12,13]. Moreover, mine tailings usually retain a certain amount of target minerals due to differences in beneficiation processes. Hence, the corresponding material properties can be obtained. Graphite tailings (GTs) are mine tailings with rich production. These are graphite components maintained after beneficiation and essentially carbon-based materials, showing certain conductive abilities [14,15]. These unique conductive abilities endow them with the potential to be developed into functional materials for EMW absorption. GTs are used as conductive admixtures in cement-based materials to enhance the EMW-absorption capacity of the latter, which is vital for consuming solid waste, reducing environmental pollution, and alleviating electromagnetic pollution that affects human health [14,16]. Liu et al. [17] prepared conductive concrete using GTs and studied the compressive strength and electrical conductivity of the conductive concrete through experiments. The results showed that the GT-based conductive concrete exhibited good mechanical strength, and the resistivity of the concrete was significantly reduced with an increase in the GT content. Bai et al. [18] prepared graphite-based foam concrete using foam concrete as a matrix and graphite as an absorber and studied the effect of the graphite content on the mechanical strength and EMW-absorption properties of the concrete. The results showed that when the graphite content was 10 wt.%, the mechanical strength and EMW-absorption ability of the foam concrete were enhanced. When the concrete thickness was 10 mm, the minimum reflection loss (RL) was −24.08 dB and the effective bandwidth was 0.466 GHz. In summary, graphite can endow cement-based materials with electrical conductivity and induce EMW-absorption properties in a certain frequency range. However, given that modern EMW-absorbing materials need to be "thin, light, strong, and wide", preparing ideal EMW-absorbing materials using only graphite as a component in cement-based materials is difficult [19,20]. Moreover, the excessive use of graphite or other low-activity additives in cement-based materials can easily lead to a significant reduction in the mechanical properties [21,22]. Therefore, an EMW-absorbing reinforcement material that is more suitable for cement-based materials should be developed to obtain an EMW-absorbing materials with excellent comprehensive performance.

Fiber is a type of toughening material, which commonly used in cement-based manterial [23,24]. Among them, steel fiber (SF) is a fiber material with excellent mechanical properties and electrical conductivity. It is often used as an EMW-absorbing reinforcement agent to prepare cement-based EMW-absorbing materials [25,26]. Li et al. [25] prepared cement-based EMW-absorbing materials using iron tailings and steel slag as filling materials and SF as an absorber. The results showed that SF increases the RL of materials while reducing their thickness. Si et al. [27] prepared a cement-based composite material using carbon black, graphite, and SF. Results proved that the addition of carbon black and SF improved the EMW-absorption performance of the graphite–cement composite material. The RL of the material with 2% carbon black and 10% SF was less than −5 dB in the frequency range of 6–18 GHz. According to the above mentioned research results, SF has a significant improvement effect on the EMW-absorption function of cement-based materials. Thus, it is necessary to explore the synergy of the EMW-absorption-improvement effect of SF and conductivity induced by GTs in cement-based materials.

In this study, cement-based EMW-absorbing materials with good EMW-absorption performance and a simple preparation process were prepared using GTs as a conductive admixture and SF as an EMW absorber. First, the mechanical and electrical properties

of the cement-based materials were measured, and a GT–cement matrix with good basic properties was obtained. Second, by adjusting the content of SF, the corresponding loss attenuation and impedance matching performance of the materials were calculated based on their electromagnetic parameters. Finally, the mechanical properties, electrical conductivity, and EMW-absorption properties of the cement-based materials and the influence mechanisms of the synergistic effect of the GTs and SFs on these properties were analyzed and discussed. This study provides a scientific design idea for preparing cement-based EMW-absorbing materials and has certain significance for preventing and controlling electromagnetic radiation pollution in urban spaces.

2. Experimental

2.1. Raw Material

The GTs were obtained from a graphite mine in Fujian Province, China. GTs are industrial wastes produced during the refining process of the graphite ore. The chemical composition of the GTs was determined by X-ray fluorescence. The main chemical components were SiO_2, Fe_2O_3, and Al_2O_3. The specific chemical composition is shown in Table 2. The particle-size distribution of the GTs was measured using a laser particle-size analyzer. The average diameter (D50) was 8.99 μm, and the particle-size distribution is shown in Figure 1. The morphology was observed by scanning electron microscopy (SEM) (Figure 2). As shown in the figure, the GTs appear as flakes. According to the Chinese standard JC/T 2572-2020 [28]. The carbon content in the GTs was determined by a high-frequency infrared absorption method; the carbon content was 19.94% of the total mass of the GTs. The test cement used was P.O 42.5 ordinary Portland cement, which was obtained from China Jiangxi Province Wannianqing Cement Co., Ltd., Nanchang, China. The chemical composition and basic performance parameters of the cement are shown in Tables 2 and 3, respectively.

Table 2. Chemical composition of the cement and GTs.

Raw Material	Component Content/%								
	SiO_2	Fe_2O_3	CaO	Al_2O_3	SO_3	MgO	TiO_2	K_2O	MnO_2
Cement	24.45	3.02	63.06	4.14	1.31	1.43	—	1.14	—
GTs	64.70	9.07	0.84	17.40	1.01	1.47	0.99	3.30	0.15

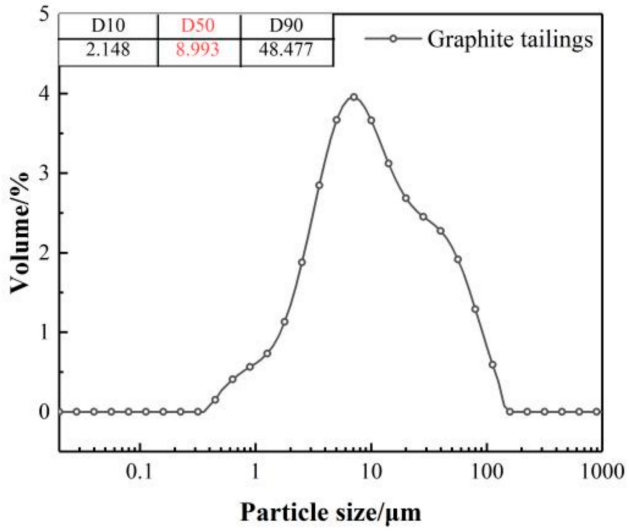


Figure 1. Particle-size distribution of the GTs.

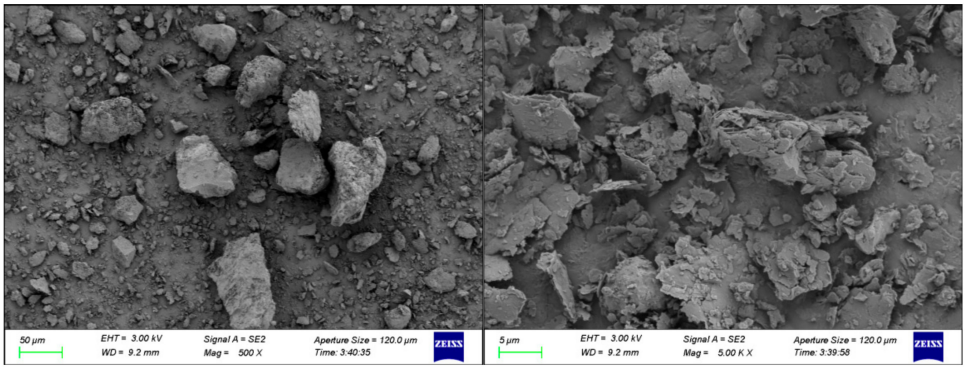


Figure 2. Morphology of the GTs with different magnifications (×500 and ×5000).

Table 3. Basic performance parameters of the cement.

Specific Surface Area/$m^2 \cdot kg^{-1}$	Setting Time/min		Stability	Compressive Strength/MPa	
	Initial	Final	Boiling Process	3 d	28 d
362	196	251	Qualified	27.7	51.2

2.2. Testing Methods

2.2.1. Sample Mixing Ratio

The cement-based materials were prepared according to the Chinese standard GB/T 17671-2021 [29]. GTs were used to replace cement, with replacement mass ratios of 0%, 10%, 20%, 30%, and 40%, and the mixing proportions were listed in Table 4. These samples were referred to as blank, G10, G20, G30, and G40, respectively. The binder–sand ratio was 1:3, and the water–binder ratio was 1:2.

Table 4. Mixing proportions of the cement-based materials.

Sample	Cement/g	GTs/g	Water–Binder Ratio	Binder–Sand Ratio
Blank	450	0	1:2	1:3
G10	405	45		
G20	360	90		
G30	315	135		
G40	270	180		

2.2.2. Specimen Preparation

During sample preparation, GTs, cement, and sand were first premixed at a low speed in a mixer for about 60 s. Then, water was added to the mixer, followed by stirring at a low speed for 60 s and then at a high speed for 120 s. Next, the mortar mixture was poured into a 40 mm × 40 mm × 160 mm steel mold and compacted on a vibrating table for 60 s. After 24 h of natural placement, the test mold was removed and placed in a standard curing room (20 °C; relative humidity = 95%) for aging. Thereafter, the performance test was conducted. The mixing proportions of paste samples used for microscopic tests were the same as those of the mortar but without sand. The paste samples were cured in the standard curing room under the same conditions as mortar samples.

2.3. Performance Testing

2.3.1. Mechanical Property Test

According to the Chinese standard GB/T 17671-2021, the flexural and compressive strengths of the specimens after 3 and 28 d of standard curing were tested using a microcomputer-controlled press-folding machine (DYE-300). The specimen size was 40 mm × 40 mm × 160 mm, loading speed of compressive strength was set to 2.4 kN/s, and loading speed of flexural strength was 0.05 kN/s. Three and six specimens were

selected for compressive and flexural strength testing at each aging duration, respectively, and the average value was calculated.

2.3.2. Electrical Property Test

The resistivity of the samples was measured using a digital bridge tester. The test frequency was 10 HZ, and the test method was a two-electrode method. The size of the test specimens was 40 mm × 40 mm × 160 mm. During the pouring and forming of the test samples, two pieces of pure copper sheets with a size of 30 mm × 40 mm were placed in the interior of the test specimens at approximately 30 mm from both ends. After standard curing for 28 d, the samples were air-dried at 60 °C for 2 h in an oven. Then, the resistivity test was performed at a constant temperature room (20 °C ± 1 °C). According to the related literature [30], the resistivity value was calculated using Equation (1):

$$\rho = \frac{R \cdot S}{L} \tag{1}$$

where R is the resistance of the test sample, L is the distance between the two copper sheets, and S represents the contact area between the copper sheets and the sample.

2.3.3. Micromorphology Testing

X-ray diffraction (XRD; Bruker D8 advanced) was used to analyze the phase composition of the hydration products. The scanning range was 5°–70° (2θ), and the scanning rate was 2°/min. The microstructure of the hydration products was analyzed by SEM (SU8600, Titachi, Japan) integrated with EDS, and surface scanning was conducted using an EDS analyzer to evaluate the distribution of elements in the hydration products. Prior to testing, the paste samples cured for specific ages were broken into small pieces, placed in anhydrous ethanol to terminate hydration, and dried in an oven at 60 °C for 2 h. Further, block samples were used for SEM testing, and remaining samples were ground into a powder in a grinding bowl and passed through a 75-μm standard sieve. The powder was used for XRD analysis.

2.3.4. Electromagnetic Parameters and EMW-Absorption Performance

The electromagnetic parameters of the samples after 28 d of curing were tested using a vector network analyzer (produced by 24 Institute of Electric Power of China). The test frequency range was 0.1–5 GHz, and the test method was the coaxial transmission method. The test specimens were circular, with an outer diameter of 23.15 mm, an inner diameter of 10.05 mm, and a height of 20 mm. Prior to testing, the samples were dried at 60 °C for 2 h to eliminate the influence of internal free water on the results of electromagnetic parameter testing. According to transmission line theory and based on the test results of the electromagnetic parameters [6,11,31], the loss attenuation coefficient, normalized impedance, and RL values of the cement-based materials were calculated. The corresponding expressions are shown in Equations (2)–(4):

$$\alpha = \frac{\sqrt{2}\pi f}{c} \times \sqrt{(\mu''\varepsilon'' - \mu'\varepsilon') + \sqrt{(\mu''\varepsilon'' - \mu'\varepsilon')^2 + (\mu''\varepsilon'' + \mu'\varepsilon')^2}} \tag{2}$$

$$Z = \frac{Z_{\text{in}}}{Z_0} = \sqrt{\frac{\mu_r}{\varepsilon_r}} \tan\left(j\frac{2\pi f d}{c}\sqrt{\mu_r \varepsilon_r}\right) \tag{3}$$

$$RL = 20\log\left|\frac{Z_{\text{in}} - Z_0}{Z_{\text{in}} + Z_0}\right| \tag{4}$$

where Z_{in} is the input impedance of the material's surface; Z_0 is the impedance of the free space; f is the frequency of the EMW; c is the velocity of light; RL is the reflection loss; ε' μ' refers to the real parts of the permittivity and permeability, respectively; and ε'' and μ'' are the imaginary parts of the permittivity and permeability, respectively.

3. Results

3.1. Mechanical and Electrical Properties of the Cement-Based Materials

Figure 3a,b show the compressive and flexural strength test results of the cement-based materials with different GT contents. The compressive and flexural strengths of the specimens after 3 and 28 d gradually decreased with increasing GT content, showing different degrees of reduction. Among the samples, we observed that when the GT content exceeded 30%, the mechanical properties of the cement-based material decreased more significantly compared to samples with less GT content. This result is mainly because GTs are low-activity materials. Furthermore, as the GT content increases, a greater proportion of cement is substituted with GT, which reduces the quantity of cement hydration products and particularly delays the formation of the early microstructure. This phenomenon can be explained by the dilution effect [32]. Results reported in the literature and those obtained in this study (Figure 2) indicate that graphite particles in GTs have a lamellar structure and high lubricity [33]. These properties easily lead to weak bonding in cement–stone structures. This phenomenon is detrimental to the mechanical properties of the cement-based materials.

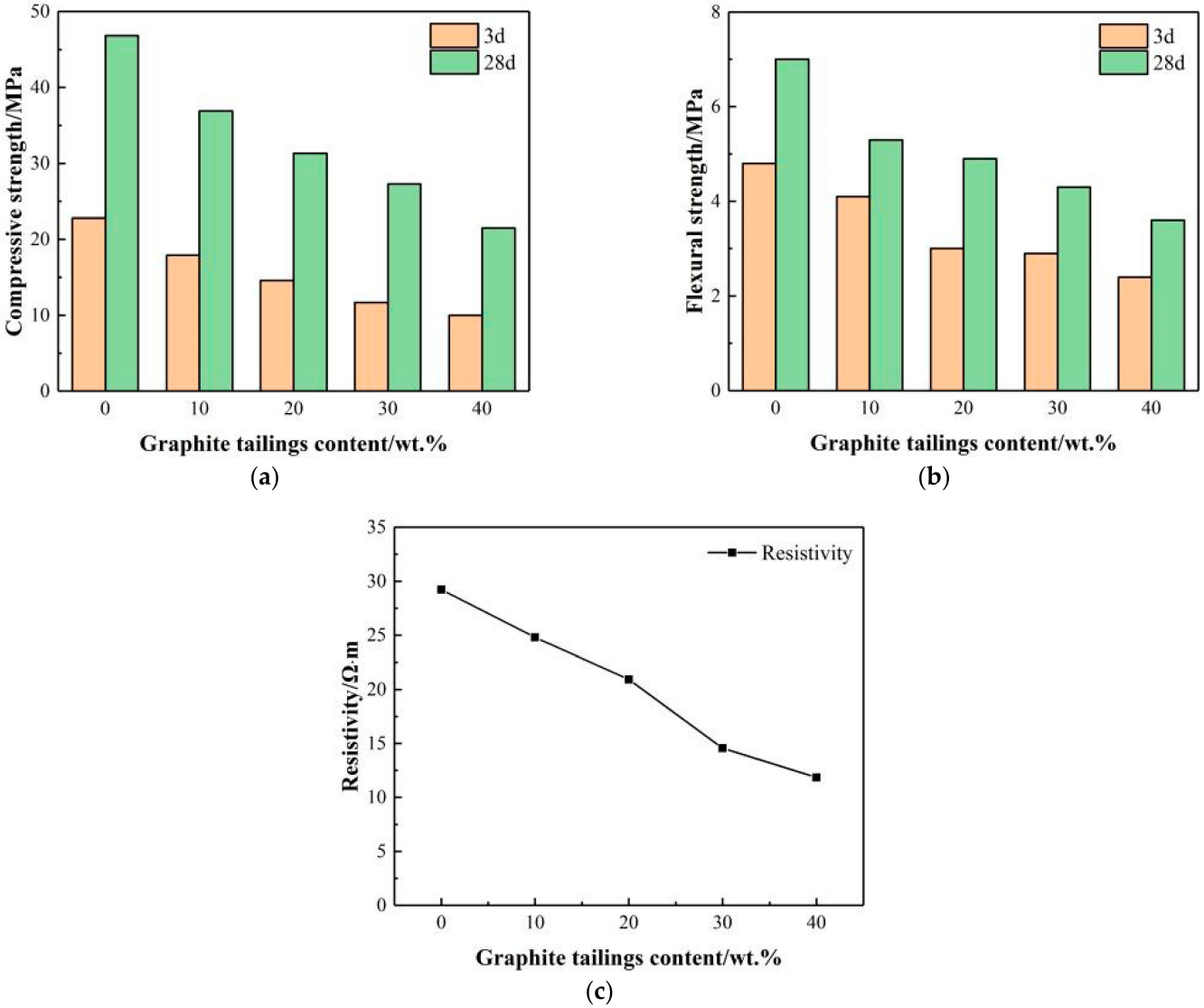


Figure 3. Strength and resistivity of the cement-based materials: (**a**) compressive strength, (**b**) flexural strength, and (**c**) resistivity.

The resistivity value reflects the resistance loss ability of a material, which is an important factor affecting the EMW-absorption performance of materials. Figure 3c shows the resistivity test results of the cement-based materials with different GT contents. The resistivity decreases with increasing content of GTs. The resistivity reaches the lowest value of 11.84 Ω·m at 40% GT content, which is 59.6% lower than that of the blank. However, when the GT content exceeds 30%, the effectiveness of enhancing the conductivity of the cement matrix diminishes, as indicated by the decreasing slope of the broken line. This finding proves that GTs can improve the conductivity of cement-based materials. This phenomenon can be explained by the tunneling effect: when electrons obtain sufficient energy, crossing a barrier becomes easier and electron transition occurs from one conductor to another to elicit conductivity [34]. Therefore, with an increase in the GT content, the spacing between graphite particles with conductivity decreases, which reduces the barrier formed by the cement matrix. Ultimately, the ability of the materials to conduct current increases.

3.2. XRD Analysis

XRD tests were conducted on the paste samples cured for 3 and 28 d, as shown in Figure 4, to investigate the effect of different GT contents on the hydration products of the cement mortar. The XRD results showed that the mineral composition of the samples at 3 and 28 d was the same; the samples contained $Ca(OH)_2$, SiO_2, $CaCO_3$, C_3S, C_2S, Al-phase hydrates, and AFt.

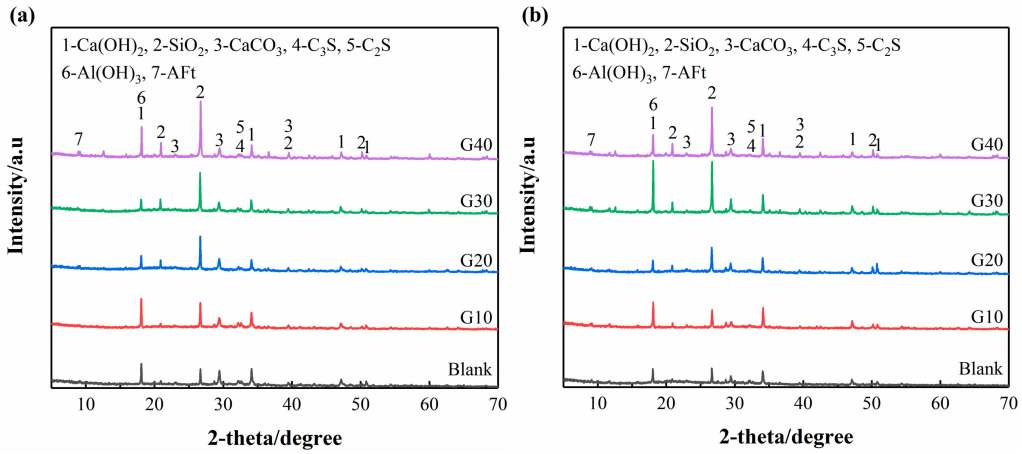


Figure 4. XRD patterns of the cement-based materials at (**a**) 3 and (**b**) 28 d.

At a hydration age of 3 d, peaks of C_3S and C_2S were observed for the blank sample, which indicated that the cement was not fully hydrated. The peak intensities of C_3S and C_2S decreased with increasing content of GTs, and the diffraction peak strength of $Ca(OH)_2$ ($2\theta = 34°$) also decreased with an increase in the content of GTs. These phenomena can be explained by the dilution effect: a large amount of GTs replace the cement particles, which leads to a decrease in the amount of cement involved in hydration [35,36]. The XRD results and the compressive strength trend of the cement-based materials at 3 d indicate that the dilution effect is the main reason for the decrease in the compressive strength.

At a hydration age of 28 d, the significant weakening of the diffraction peaks of C_3S and C_2S indicated that the cement underwent sufficient hydration. Moreover, the diffraction peak of $Ca(OH)_2$ first increased and then decreased with increasing GT content. This may be because the particle size of GTs is small and an appropriate dosage can effectively realize microaggregate filling and the nucleation effect [36,37], which promotes the hydration of the cement. Generally, enhancing the compactness of cement-based materials is advantageous, as it diminishes the penetration pathways and reduces the proportion of detrimental pores. These improvements contribute to the durability and hydration stability of the material to some extent [38]. In addition, the peak of SiO_2 intensifies with increasing GT content at a curing age of 28 d, which is consistent with the result observed for a hydration age of

3 d. According to the relevant literature [33,39,40], quartz existing in the GTs is inert, which means that the volcanic ash reaction does not occur under normal circumstances. Therefore, the peak of SiO_2 intensifies with increasing content of GTs. Notably, the high content of Al_2O_3 in GTs enables them to react with gypsum in the cement, which also explains the high content of AFt observed in the test samples with high GT content.

3.3. SEM and EDS Analysis

The cement mortar samples cured for 3 and 28 d were tested by SEM to investigate the effect of different GT contents on the hydration products of the cement mortar. The SEM images are shown in Figures 5 and 6.

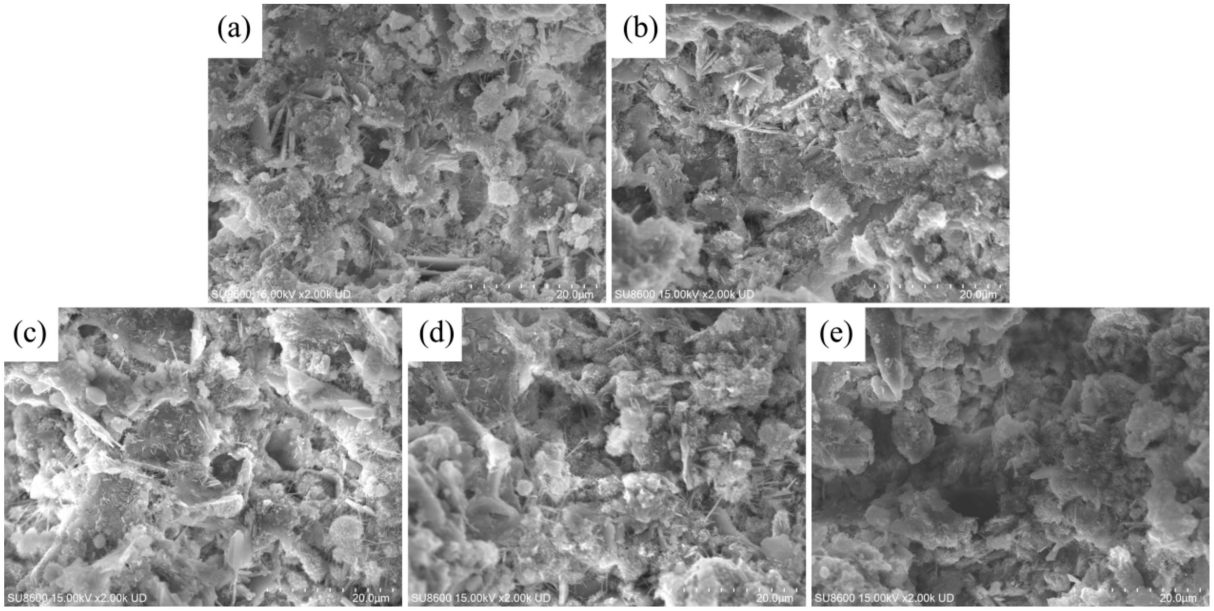


Figure 5. SEM images of the cement-based materials cured for 3 d: (**a**) Blank, (**b**) G10, (**c**) G20, (**d**) G30, and (**e**) G40.

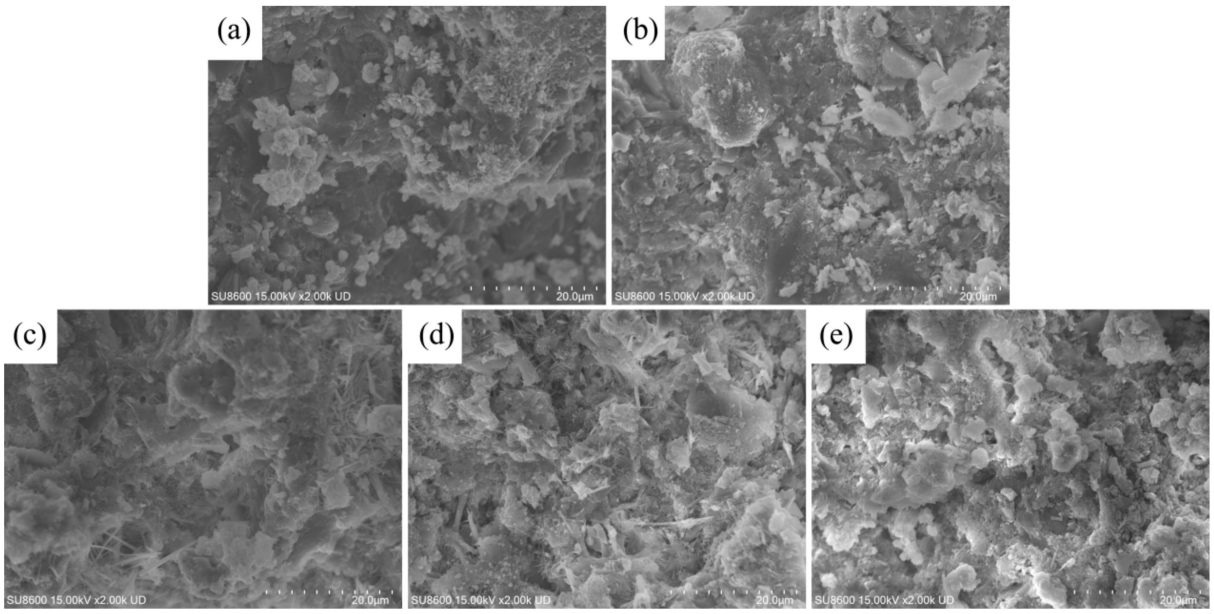


Figure 6. SEM images of the cement-based materials cured for 28 d: (**a**) Blank, (**b**) G10, (**c**) G20, (**d**) G30, and (**e**) G40.

Figure 5 shows the SEM image of the cement-based sample cured for 3 d. At the age of 3 d, the insufficient hydration of the cementitious material system reduces the surface compactness and loosens the structure of the hydration products. Furthermore, an increase in the GT content is not conducive to the densification of sample microstructure, which is consistent with the declination trend of the early strength of the samples. Figure 6 shows that the cementitious material system undergoes sufficient hydration after 28 days and a large amount of the C–S–H gel and AFt are generated, which is consistent with the XRD results. In addition, the compactness of the sample microstructure is greatly improved, which is beneficial for the development of the later strength of the samples.

The G30 sample cured for 28 days was selected for the EDS energy spectrum analysis to analyze its elemental composition. The results of EDS surface scanning are shown in Figure 7. In the G30 sample, C, Ca, Si, Al, and Fe were the main elements of the hydration products. Among them, Ca, Si, and Al are the main chemical elements of the hydration products of Portland cement, such as C–S–H, AFt, $Ca(OH)_2$, and $CaCO_3$. Additionally, the presence of a large amount of C and Fe was mainly attributed to the addition of GTs. The results of the surface scanning showed that the dispersion of C and Fe was uniform, which indicated that graphite particles and Fe-phase minerals were well dispersed in the cement matrix. This enhanced the electrical conductivity of the matrix material to a certain extent, which is consistent with the results observed in Section 2.1.

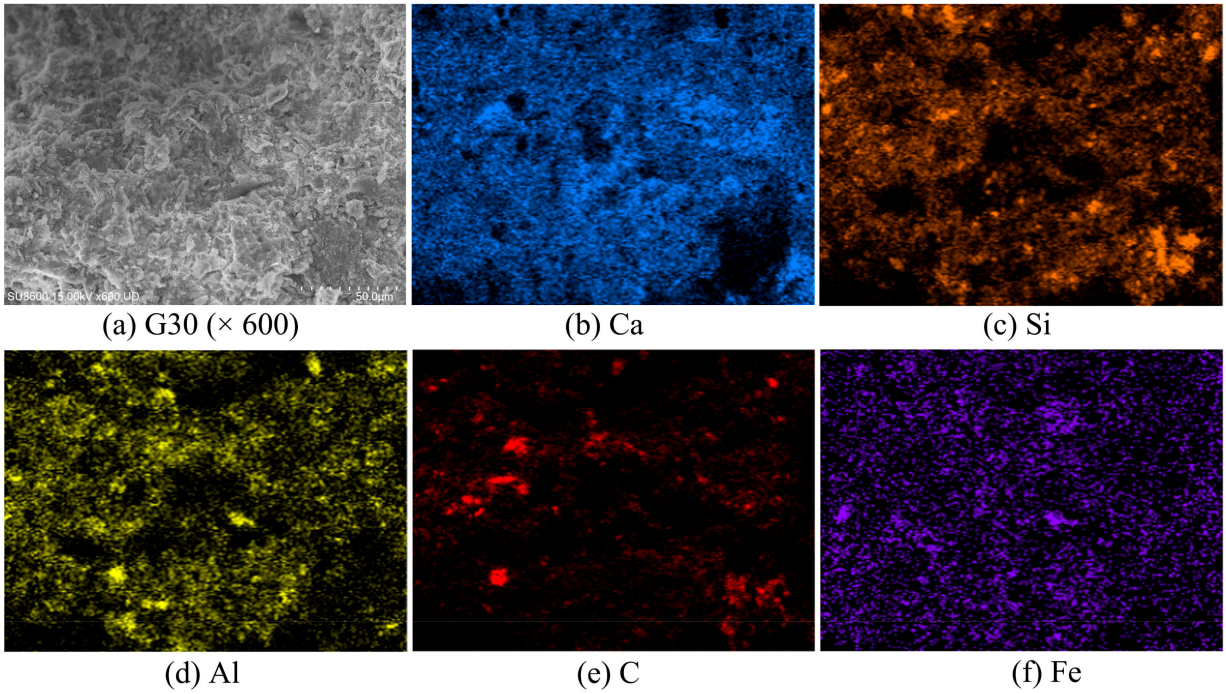


Figure 7. EDS results of the cement-based materials.

3.4. Preparation of the Cement-Based EMW-Absorbing Materials with GTs and SF

3.4.1. Mixing Proportions of the EMW-Absorbing Materials

As reported in Sections 2.1–2.3, the mechanical and electrical properties of the cement-based materials were comprehensively evaluated. When the content of GTs was 30%, the cement-based materials showed excellent mechanical and electrical properties. This content was more beneficial to the consumption of solid waste. On this basis, cement-based EMW-absorbing materials with GTs and SF were prepared by adding SF with mass ratios of 2%, 4%, 6%, and 8% considering the total mass of the cementitious materials. The specific mixing proportions are shown in Table 5.

Figure 8a,b show the test results of the compressive and flexural strengths of the cement-based materials with different SF contents. The figures show that the compressive

and flexural strengths after 3 d were improved after SF incorporation. Moreover, the flexural strength after curing for 28 d was slightly improved, while the compressive strength after curing for 28 d did not change considerably. The effect of SF on the flexural strength of the cement-based materials was more obvious. This was because SF is a ductile material with high tensile strength and was distributed in cement-based materials in multiple directions. This effectively delayed the development of cracks and improved the tensile and flexural strengths of the materials.

Table 5. Mixing proportions of the cement-based EMW-absorbing materials with GTs and SF.

Sample	Cement/g	GTs/g	Water–Binder	Binder–Sand	SF/g
G30-1	315	135	1:2	1:3	9 (2%)
G30-2	315	135			18 (4%)
G30-3	315	135			27 (6%)
G30-4	315	135			36 (8%)

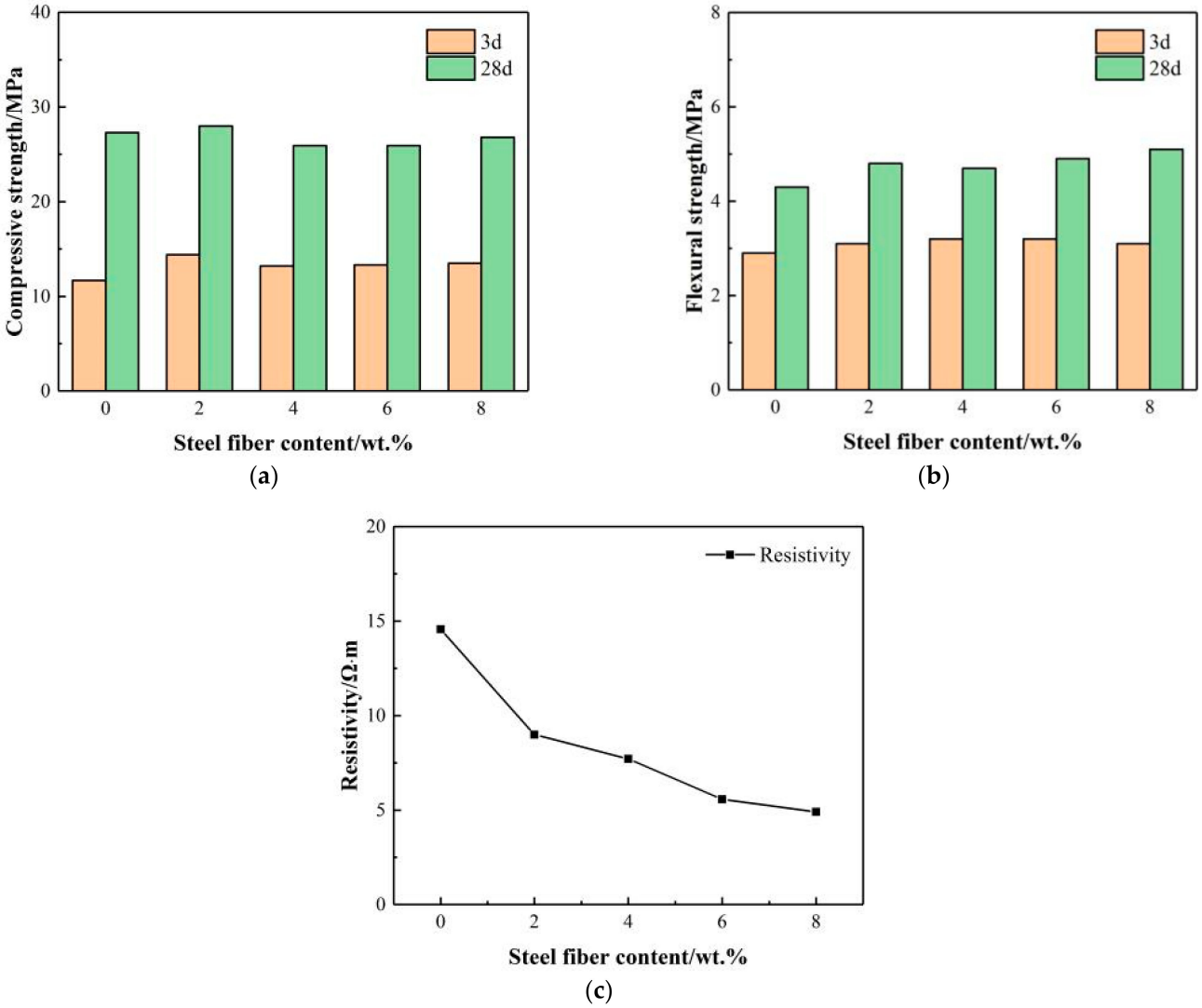


Figure 8. Strength and resistivity of the cement-based materials containing GTs and SF: (**a**) compressive strength, (**b**) flexural strength, and (**c**) resistivity.

Figure 8c shows the resistivity test results of the cement-based materials with different SF contents. As shown in the figure, the resistivity decreases with increasing SF content. The resistivity reaches the lowest value of 4.9 Ω·m when the SF content is 8%. This result

is mainly because with an increase in the SF content, SF in the cement-based materials becomes densely distributed and SF easily overlaps to form a conductive network, reducing the resistivity value. However, the decrease in the resistivity gradually tends to be gentle after the SF content exceeds 6%; that is, the resistivity of the cement-based materials reaches a percolation threshold [41]. At this time, the dosage efficiency of SF reaches the highest. As per the resistivity test results of the cement-based materials reported in Section 2.1, GTs are dispersed in the cement-based materials as a conductive admixture. This increases the probability of contact between SF and GTs, thus enhancing the conductivity of the materials.

3.5. EMW-Absorption Properties

3.5.1. Analysis of Electromagnetic Parameters

Electromagnetic parameters are characteristic parameters describing the interaction between materials and electromagnetic fields, which play a crucial role in the EMW-absorption properties of materials. Figure 9a,b show the real (ε') and imaginary parts (ε'') of the complex permittivity of the cement-based materials with different SF contents, respectively. ε' is used to describe the ability of materials to store electrical energy, and ε'' is used to describe the ability of materials to lose electrical energy. Figure 9a shows that the ε' value of the blank group remains unchanged when the test frequency changes. After the material is mixed with SF, the ratio of ε' to the blank sample increases, and it increases with increasing SF content. Among the samples, the G30-3 and G30-4 samples show higher ε' values, indicating that they have stronger abilities to store electric energy. Figure 9b shows that the ε'' value of the blank group is close to 0, which means that it has a very weak electrical loss capability. After the incorporation of SF, the ε'' value of the materials increases, which implies that SF improves the electrical loss capacity of the materials. Further, G30-1, G30-2, and G30-3 show a peak between the test frequency of 2–3 GHz, indicating that the samples have the strongest electrical loss capability in this frequency range. Notably, the ε'' value of the G30-4 sample is lower than that of the other samples at 0–3 GHz; however, the value is higher in the frequency range of 3–5 GHz. Further, the value has a tendency to move to high frequency, which indicates that the sample has a high power loss ability in the high-frequency region.

Figure 9c,d show the real part (μ') and imaginary part (μ'') of the complex permeability of the cement-based materials with different SF contents. μ' represents the ability of a material to store magnetic energy, and μ'' represents the ability of a material to lose magnetic energy. As shown in Figure 9c, the μ' value of the blank sample fluctuates at around 1 and increases slightly after adding SF. A small peak is observed in the test frequency range of 2–3 GHz, which indicates the highest magnetic-energy storage capacity of the sample in this frequency range. As shown in Figure 9d, the μ'' value of the blank sample fluctuates at around 0, which suggests that pure cement does not have magnetic-loss capability. After adding SF, the μ'' value of the cement-based materials slightly increases and a small peak is observed between 2 and 3 GHz. This implies that the magnetic-loss capacity is the highest in this frequency range for the samples. The reason for this phenomenon is that SF shows ferromagnetism, which produces a certain electromagnetic loss effect [42]. Furthermore, GTs have some magnetic substances such as hematite and magnetite, which can cooperate with the electromagnetic loss ability of SF-reinforced materials to improve EMWs' loss ability. Notably, the μ'' value of the G30-4 sample is lower than those of the G30-2 and G30-3 samples. This distinct test result may be because its magnetic-loss frequency band moves to a higher frequency band (>5 GHz).

3.5.2. Loss Attenuation

The EMW-absorption capacity of materials is expressed by the loss attenuation coefficient α. A larger α value means a stronger loss attenuation ability of the material to EMWs in a frequency range. Figure 10 shows the α value of the cement-based materials with different SF contents. The α value of the blank sample fluctuates near 0, which indicates

that the blank sample has no loss attenuation ability to EMWs. With the addition of SF, the α value increases and the frequency band broadens, which suggests that SF enhances the EMW-absorption ability of the materials. The maximum values of α for G30-2 and G30-3 were observed in the frequency range of 2.5–3 GHz. In addition, when the SF content was less than 6%, the loss attenuation ability of the cement-based materials increased with increasing SF content. Notably, for the G30-4 sample, the loss attenuation peak has a tendency to move to the high-frequency region (>5 GHz), which indicates that the loss attenuation ability of the G30-4 sample may be higher than 5 GHz. This phenomenon is consistent with the discussion of electromagnetic parameters in Section 3.5.1. In fact, the synergistic effect of GTs and SF is a significant factor in the development of the EMW-loss mechanism in cement-based materials. The incorporation of GTs and SF enhances the conductivity of the material, thereby increasing its dielectric loss. Additionally, the presence of magnetic components, such as hematite and magnetite in GTs, along with the ferromagnetic properties of SF, contributes to the material's magnetic loss in response to EMWs. This synergistic effect results in an improved loss attenuation coefficient, which is advantageous for enhancing the EMW-absorbing properties of the material.

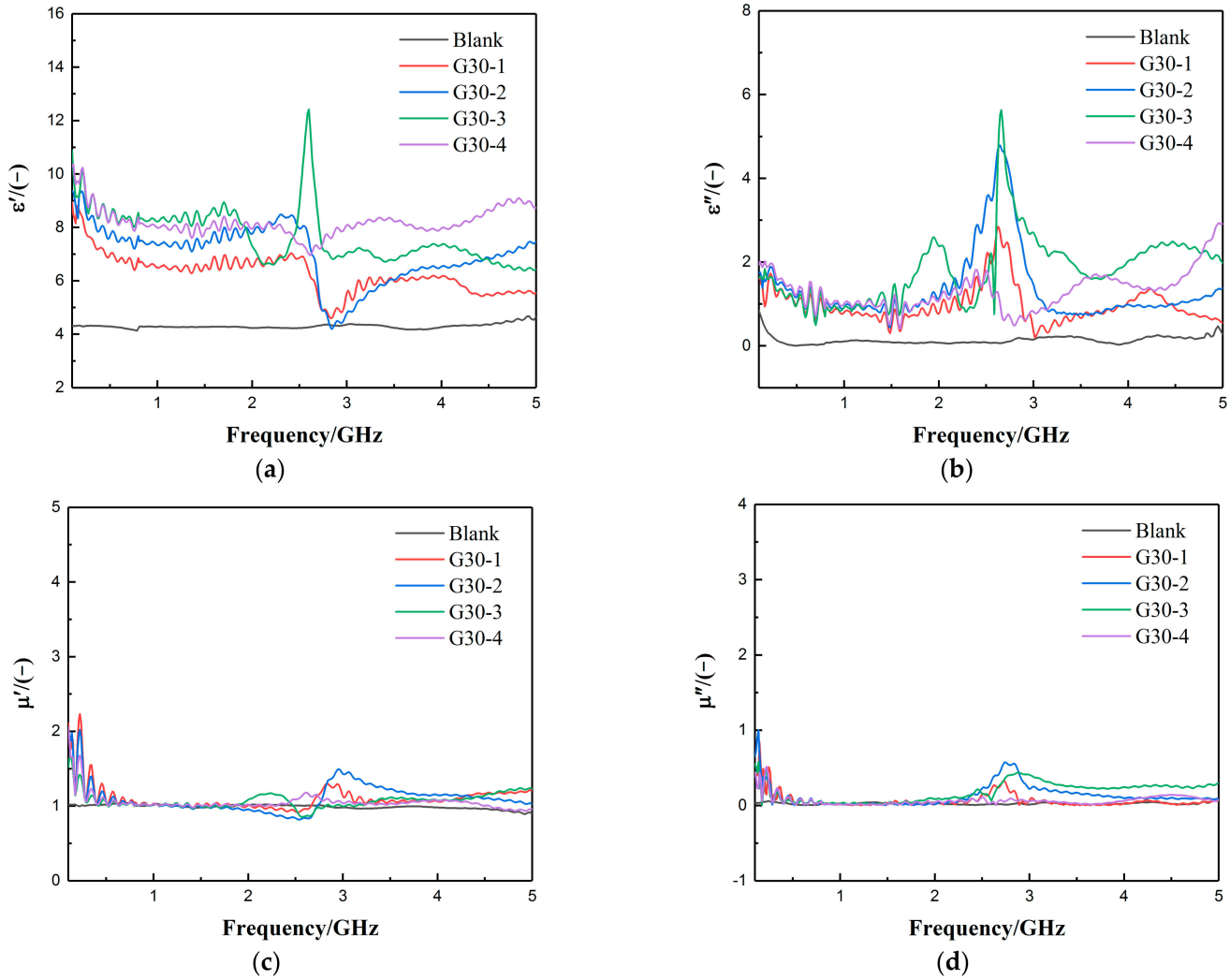


Figure 9. Electromagnetic parameters of the cement-based materials with different SF contents: (**a**) ε', (**b**) ε'', (**c**) μ', and (**d**) μ''.

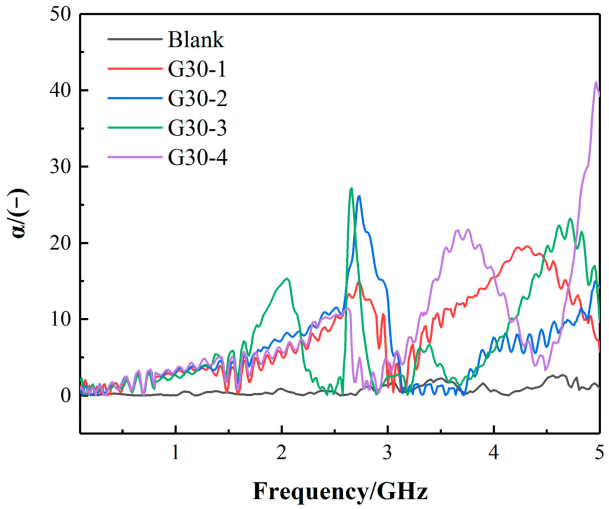


Figure 10. Attenuation coefficient of the cement-based materials with different SF contents.

3.5.3. Impedance Matching

EMW-absorbing materials should have good impedance matching characteristics, i.e., the impedances of an EMW-absorbing material matrix and air should be as similar as possible. Therefore, in the design of EMW-absorbing materials, incident EMWs should enter the materials to the greatest extent and attenuate the loss of EMWs in the materials as much as possible, rather than reflecting on the surface of the material [9,43]. According to the transmission line theory [6,11,31], as shown in Equation (2), the characteristic impedance can be calculated from electromagnetic parameters. Moreover, the normalized impedance value can be calculated from the characteristic impedance of air.

Figure 11 shows the normalized impedance matching values of the cement-based materials with different SF contents. The normalized impedance matching value of the blank sample is the highest, which implies that the impedance matching between the pure mortar sample and the free space is the worst. This phenomenon was also observed in the related literature [44,45]. After the incorporation of GTs and SF, the impedance matching of the materials is significantly improved, which increases the possibility of EMWs entering the materials. This improvement is attributed to the synergistic effect of GTs and SF on the materials. According to previous research [27,34,46], the main factors of this synergistic effect can be summarized as follows: (1) GTs contain a large amount of quartz and other mineral components. The mineral components with a low dielectric constant reduce the real part of the complex dielectric constant of the cement-based materials. Consequently, the impedance matching of the materials and free space is improved, which is conducive to EMWs entering the materials. (2) An appropriate amount of SF enables the materials to show good impedance-matching characteristics by adjusting their electromagnetic parameters. However, excessive SF content makes the material conductivity considerably high, which causes a large amount of reflection of EMWs on the surface of the materials. Ultimately, the impedance matching characteristics deteriorate (such as that in the case of G30-4).

3.5.4. RL Value

The EMW-absorption performance of the materials was evaluated through RL. The minimum value of RL and the effective bandwidth (less than or equal to −10 dB) jointly determine the strength of the EMW-absorption performance of materials. According to JGJ/T 220-2010 [47], the total thickness of building plastering mortar is usually 15–25 mm. The samples were prepared with a reference thickness of 20 mm to meet these design requirements, and their RL values and effective bandwidths were measured.

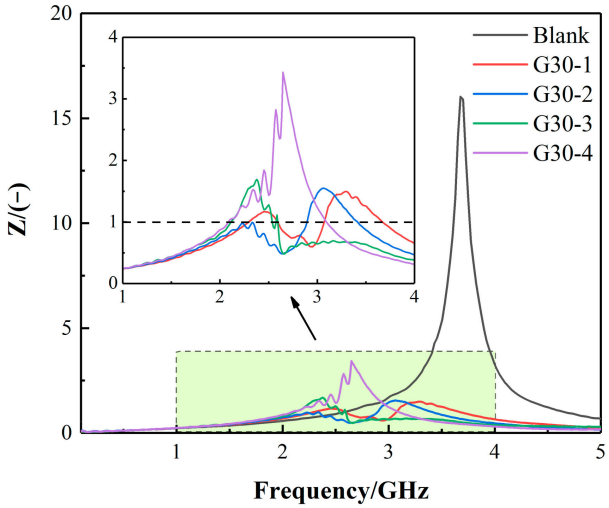


Figure 11. Normalized impedance matching values of the cement-based materials with different SF contents.

Figure 12 shows the RL values and effective bandwidths of the cement-based materials with different SF contents. As shown in Figure 12a, each sample mixed with GTs and SFs exhibited good EMW-absorption properties. When the content of GTs was 30% and the content of SF increased from 2% to 6%, the RL value and effective bandwidth gradually increased. Therefore, SF has a positive effect on improving the EMW-absorption performance of the materials. Notably, the G30-3 sample with 30% GT and 6% SF showed the maximum absorption peak at 2.54 GHz and its minimum RL and effective bandwidth were −25.78 dB and 0.953 GHz, respectively. However, the minimum RL value of the G30-4 sample was −11.95 dB and the effective bandwidth decreased to 0.06 GHz. This significant reduction was mainly due to the excessive content of SF. The conductivity was considerably high (as reported in Section 3.4.1), which caused substantial reflection of EMWs incident on the material interface; that is, the "Faraday cage" effect was observed [48]. This phenomenon eventually led to a decrease in the EMW-absorption performance of the material.

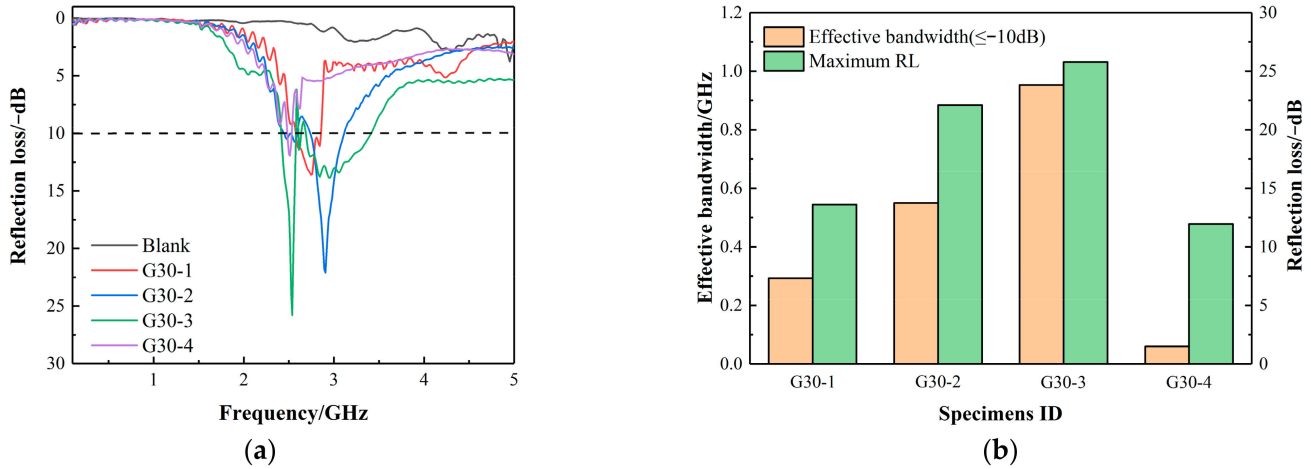


Figure 12. EMW-absorption performance of the cement-based materials with different SF contents: (**a**) RL and (**b**) minimum RL and effective bandwidth.

4. Discussion and Mechanism Analysis

This study proposes a preparation method for cement-based EMW-absorbing materials with excellent performance. These materials not only realize the resource utilization of mine solid waste but also are important for preventing and controlling EMW pollution in urban spaces. From the perspective of the preparation of cement-based materials, the high-volume

use of GTs yields significant green benefits. Table 6 presents a comparison of cement-based materials with various additives as reported in the recent literature. Moreover, SF enhances the mechanical and EMW-absorption properties of cement-based materials, which is vital for the high-performance development of functional building materials. In the EMW-absorbing materials, GTs improve the current transmission capacity of the cement-based material matrix and SFs construct a complete conductive network. The two components synergistically enhance the electrical loss capacity of the cement-based materials, which improves their absorption capacity for EMWs. Considering the practical application of these materials, their proposed preparation method is simple: adjusting the content of GTs and SF yields good material performance, more convenient for the actual construction operation. Moreover, the cement-based materials show good EMW-absorption capacity at a thickness of 20 mm. The strength grades of the materials can reach the requirements of M25 cement plastering mortar, fully meeting the design requirements of cement plastering mortar as per the industry standard JGJ/T 220-2010. In this study, XRD and SEM/EDS methods were employed to characterize the phase evolution of the cement matrix containing GTs. The application of micro-level computational techniques, such as molecular dynamics and density functional theory, can provide a more comprehensive understanding of the properties of cementitious materials enhanced by nano-micron additives like GTs [49]. Future research will focus on deepening our understanding of these computational methods and integrating them into our ongoing investigations to gain a more complete insight into the performance evolution characteristics of cement-based materials.

Figure 13 shows the transmission loss mechanism of the cement-based materials with GTs and SF for EMWs. The EMW-absorption mechanism of the cement-based materials can be explained considering two aspects: the impedance matching ability and electrical loss ability. In terms of impedance matching, GTs and SF synergistically adjust the electromagnetic parameters of the cement-based materials, reducing the impedance between the free space and the materials. Consequently, more EMWs enter the materials. With regard to the electrical loss capacity, GTs are uniformly dispersed in the cement-based materials and lead to effective multiple reflections of EMWs and dipole polarization [50,51]. Moreover, numerous "microcapacitors" are formed between GT particles [52], which can improve the power storage capacity of the materials (that is, the real part of the complex permittivity of the cement-based materials is enhanced). The overlap between SFs gradually forms a complete conductive network, and an increase in the SF content increases the real part of the complex permittivity to varying degrees. This phenomenon can be explained as a controlling effect of a conductive fiber on the dielectric properties of a material. Under the synergistic effect of GTs and SF, a good resistance loss mechanism is observed in cement-based materials. Thus, the cement-based materials with GTs and SF show excellent EMW-absorption performance under the synergistic effect of the two components.

Table 6. Comparison of cement-based materials with EMW-absorbing properties in the recently reported literature.

Additives	Thickness/mm	RL_{min}/dB	Effective Bandwidth/GHz	References
None	15	−12.67	1.85 (below −6dB)	[20]
KH550@Fe_3O_4	35	>−12.50	14.8	[53]
Carbon black	10	−25.52	1.87	[6]
Expanded polystyrene	60	−19.00	16.9	[54]
Carbon fiber	30	>−13.00	5.20	[31]
GTs and SF	20	−25.78	0.953	This work

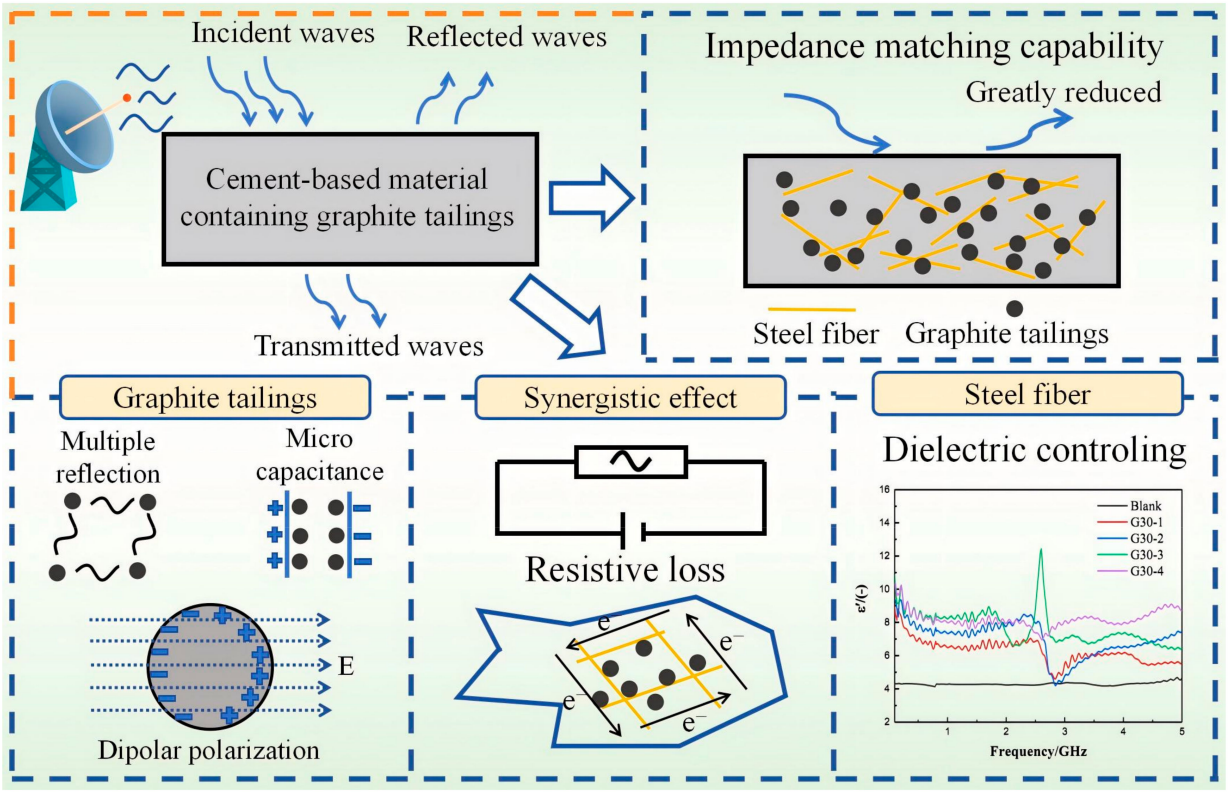


Figure 13. Schematic of the transmission loss mechanisms of the cement-based materials containing GTs and SF.

5. Conclusions

Herein, a simple preparation method for cement-based EMW-absorbing materials with good performance is proposed. The EMW-absorption mechanism of the cement-based materials with GTs and SF was studied. The main conclusions were as follows:

1. The mechanical properties of the cement-based materials greatly deteriorated under the influence of dilution due to the incorporation of low-activity GTs. However, GTs contain a large amount of carbon-based conductive components, which improves the electrical conductivity of cement-based materials;
2. The hydration products of the cement-based materials were mainly $Ca(OH)_2$, SiO_2, $CaCO_3$, Al-phase hydrates, and AFt. An appropriate amount of GTs could effectively realize microaggregate filling and the nucleation effect, promoting the hydration of the cement-based materials;
3. The addition of SF to the cement-based materials slightly improved the compressive strength, and the enhancement in the flexural strength was more obvious. SF interacted with GTs to generate a more complete conductive network inside the cement-based materials, which improved the electrical conductivity of the materials;
4. GTs and SF significantly affected the electromagnetic parameters of the cement-based materials. Thus, they significantly affected the impedance matching characteristics and loss attenuation ability of the materials. The best loss attenuation ability was achieved in the frequency range of 2.5–3 GHz, with good impedance matching;
5. The EMW-absorption properties of the cement-based materials were significantly improved due to the synergistic effect of GTs and SF. When the content of GTs was 30% and the content of SF was 6%, the EMW-absorption performance of the cement-based materials with a thickness of 20 mm was the best. In the frequency range of 0.1–5 GHz, the minimum RL value was −25.78 dB and the effective bandwidth was 0.953 GHz.

Author Contributions: Conceptualization, H.L.; methodology, T.W., F.L. and H.L.; formal analysis, Q.W.; investigation, Q.W. and R.W.; resources, T.W.; data curation, D.Z.; writing—original draft preparation, R.W.; writing—review and editing, Q.W. and H.L.; visualization, F.L.; project administration, D.Z.; funding acquisition, T.W. All authors have read and agreed to the published version of the manuscript.

Funding: The authors gratefully acknowledge the financial support provided by the resource chemical industry science and technology innovation joint funding project of Nanping under Grant No. N2020Z003, transportation science and technology project of Fujian Province under Grant No. 202231, as well as students' innovation and entrepreneurship project of Fujian Province under Grant No. S202310397050.

Data Availability Statement: The raw data supporting the conclusions of this article will be made available by the authors on request.

Conflicts of Interest: The authors declare no conflicts of interest.

References

1. Guo, Y.; Ruan, K.; Wang, G.; Gu, J. Advances and mechanisms in polymer composites toward thermal conduction and electromagnetic wave absorption. *Sci. Bull.* **2023**, *68*, 1195–1212. [CrossRef]
2. Li, Q.; Zhang, Z.; Qi, L.; Liao, Q.; Kang, Z.; Zhang, Y. Toward the Application of High Frequency Electromagnetic Wave Absorption by Carbon Nanostructures. *Adv. Sci.* **2019**, *6*, 1801057. [CrossRef] [PubMed]
3. Lan, D.; Li, H.; Wang, M.; Ren, Y.; Zhang, J.; Zhang, M.; Ouyang, L.; Tang, J.; Wang, Y. Recent advances in construction strategies and multifunctional properties of flexible electromagnetic wave absorbing materials. *Mater. Res. Bull.* **2024**, *171*, 112630. [CrossRef]
4. Xie, S.; Ji, Z.; Zhu, L.; Zhang, J.; Cao, Y.; Chen, J.; Liu, R.; Wang, J. Recent progress in electromagnetic wave absorption building materials. *J. Build. Eng.* **2020**, *27*, 100963. [CrossRef]
5. Hou, S.; Wang, Y.; Gao, F.; Yang, H.; Jin, F.; Ren, L.; Wu, Q.; Ge, H.; Wang, Y. A novel approach to electromagnetic wave absorbing material design: Utilizing nano-antenna arrays for efficient electromagnetic wave capture. *Chem. Eng. J.* **2023**, *471*, 144779. [CrossRef]
6. Li, H.; Wei, M.; Song, Y.; Wang, R.; Liu, F.; Liu, F. Design and optimization of double-layer structure for improved electromagnetic wave absorbing characteristic of single-layer foam cement-based materials containing carbon black. *J. Build. Eng.* **2024**, *89*, 109319. [CrossRef]
7. Pavlík, M.; Bereš, M.; Beňa, Ľ. The Influence of Various Commonly Used Building Materials on the Shielding Effectiveness, Reflection and Absorption of the Electromagnetic Wave. *Appl. Sci.* **2024**, *14*, 2521. [CrossRef]
8. Shi, Y.; Jing, H.; Liu, B.; Qian, H. Electromagnetic (EM) wave absorption properties of cementitious building composites containing MnZn ferrite: Preferable effective bandwidth and thickness via iron and graphite addition. *J. Magn. Magn. Mater.* **2022**, *560*, 169555. [CrossRef]
9. Bian, P.; Zhan, B.; Gao, P.; Yu, Q.; Yang, Y.; Hong, L.; Zhang, W. Investigation on the electromagnetic wave absorption properties of foamed cement-based materials. *Constr. Build. Mater.* **2023**, *364*, 129903. [CrossRef]
10. Liu, X.; Wang, N.; Wang, Z. Effects of the absorber, thickness and surface roughness on the electromagnetic wave absorption characteristics of magnesium phosphate cement. *Constr. Build. Mater.* **2022**, *344*, 128149. [CrossRef]
11. Yang, Y.; Shi, X.; Zhou, Q.; Deng, G.; Li, W.; Li, C.; Yang, T.; Yin, L. Structural design and electromagnetic wave absorbing performance optimization of lightweight foam cement-based metamaterials. *Constr. Build. Mater.* **2024**, *438*, 137191. [CrossRef]
12. Yao, R.; Liao, S.; Dai, C.; Liu, Y.; Chen, X.; Zheng, F. Preparation and characterization of novel glass–ceramic tile with microwave absorption properties from iron ore tailings. *J. Magn. Magn. Mater.* **2015**, *378*, 367–375. [CrossRef]
13. Kuranchie, F.A.; Shukla, S.K.; Habibi, D.; Mohyeddin, A. Utilisation of iron ore tailings as aggregates in concrete. *Cogent Eng.* **2015**, *2*, 1083137. [CrossRef]
14. Xue, J.; Wang, X.; Wang, Z.; Xu, S.; Liu, H. Investigations on influencing factors of resistivity measurement for graphite tailings concrete. *Cem. Concr. Compos.* **2021**, *123*, 104206. [CrossRef]
15. Liu, H.; Xue, J.; Li, B.; Wang, J.; Lv, X.; Zhang, J. Effect of graphite tailings as substitute sand on mechanical properties of concrete. *Eur. J. Environ. Civ. Eng.* **2022**, *26*, 2635–2653. [CrossRef]
16. Mahmoud, A.A.; Elkatatny, S. Improving class G cement carbonation resistance for applications of geologic carbon sequestration using synthetic polypropylene fiber. *J. Nat. Gas Sci. Eng.* **2020**, *76*, 103184. [CrossRef]
17. Liu, H.; Liu, K.; Lan, Z.; Zhang, D. Mechanical and Electrical Characteristics of Graphite Tailing Concrete. *Adv. Mater. Sci. Eng.* **2018**, *2018*, 9297628. [CrossRef]
18. Bai, Y.-h.; Chen, Y.-j.; Lu, Y. Graphite-enhanced foam cement-based materials: Mechanical properties, pore structure and electromagnetic wave absorption performance. *Mater. Today Commun.* **2024**, *40*, 109377. [CrossRef]
19. Nam, I.W.; Choi, J.H.; Kim, C.G.; Lee, H.K. Fabrication and design of electromagnetic wave absorber composed of carbon nanotube-incorporated cement composites. *Compos. Struct.* **2018**, *206*, 439–447. [CrossRef]

20. Dai, Y.; Wu, J.; Wang, F.; Zhu, N.; Tang, H.; Zhang, Z. Research on electromagnetic wave absorption properties of Portland cement. *Mater. Res. Bull.* **2024**, *178*, 112903. [CrossRef]
21. Zhang, C.; Khorshidi, H.; Najafi, E.; Ghasemi, M. Fresh, mechanical and microstructural properties of alkali-activated composites incorporating nanomaterials: A comprehensive review. *J. Clean. Prod.* **2023**, *384*, 135390. [CrossRef]
22. Diao, X.; Song, Y.; Pan, S.; Cai, X.; Shi, T.; Wang, L. Enhanced dynamic compressive performance of silicon carbide whiskers-modified mortars. *Constr. Build. Mater.* **2024**, *432*, 136626. [CrossRef]
23. Elkatatny, S.; Gajbhiye, R.; Ahmed, A.; Mahmoud, A.A. Enhancing the cement quality using polypropylene fiber. *J. Pet. Explor. Prod. Technol.* **2020**, *10*, 1097–1107. [CrossRef]
24. Ahmed, A.; Mahmoud, A.A.; Elkatatny, S. The effect of polypropylene fiber on the curing time of class G oil well cement and its mechanical, petrophysical, and elastic properties. *J. Pet. Explor. Prod. Technol.* **2023**, *13*, 1181–1196. [CrossRef]
25. Li, H.; Zheng, G.; Wang, R.; Yang, H.; Zhang, Q.; He, Y. Study on the preparation and properties of iron tailings-steel slag based composite microwave absorbing materials. *Met. Mine* **2022**, *2*, 224–230.
26. Ameli, A.; Nofar, M.; Wang, S.; Park, C.B. Lightweight Polypropylene/Stainless-Steel Fiber Composite Foams with Low Percolation for Efficient Electromagnetic Interference Shielding. *ACS Appl. Mater. Interfaces* **2014**, *6*, 11091–11100. [CrossRef]
27. Si, T.; Xie, S.; Ji, Z.; Ma, C.; Wu, Z.; Wu, J.; Wang, J. Synergistic effects of carbon black and steel fibers on electromagnetic wave shielding and mechanical properties of graphite/cement composites. *J. Build. Eng.* **2022**, *45*, 103561. [CrossRef]
28. *JC/T 2572-2020*; Test Method for Fixed Carbon Content of Graphite Ore. Standardization Administration of China: Beijing, China, 2020.
29. *GB/T 17671-2021*; Test Method of Cement Mortar Strength (ISO Method). Standardization Administration of China: Beijing, China, 2021.
30. Wang, Z.; Shao, T.; Zhang, H.; Huo, J.; Liu, J.; Zhang, T.; Ji, X.; Zhang, H.; Wang, J.; Guo, H.; et al. Principles, properties and applications of smart conductive cement-based composites: A state-of-the-art review. *Constr. Build. Mater.* **2023**, *408*, 133569. [CrossRef]
31. Bian, P.; Yu, Q.; Zhan, B.; Gao, P.; Guo, B.; Hong, L.; Yang, Y.; Han, A. Enhancing electromagnetic wave absorption and flexural properties in carbon fiber-reinforced foamed cement-based composites. *Constr. Build. Mater.* **2024**, *415*, 134989. [CrossRef]
32. Huang, S.; Huo, B.; Chen, C.; Zhang, Y. The influence of metakaolin on the hydration of steam-cured steel slag blended cement. *Mater. Rep.* **2022**, *36*, 73–78.
33. Duan, H.; Liu, H.; Li, B.; Wang, Z.; Gao, H. Mechanical Properties and Mechanism Analysis of Graphite Tailings Environment-Friendly Concrete. *Materials* **2022**, *15*, 8870. [CrossRef] [PubMed]
34. Li, H.; Chen, H.; Wei, M.; Wang, R.; Lei, N.; Wang, Q. Design and preparation of double-layer iron ore tailings cement-based electromagnetic wave absorbing materials containing carbon black and steel fiber. *Constr. Build. Mater.* **2023**, *364*, 129972. [CrossRef]
35. Wang, D.; Shi, C.; Farzadnia, N.; Shi, Z.; Jia, H.; Ou, Z. A review on use of limestone powder in cement-based materials: Mechanism, hydration and microstructures. *Constr. Build. Mater.* **2018**, *181*, 659–672. [CrossRef]
36. Li, H.; Liu, F.; Pan, Z.; Li, H.; Wu, Z.; Li, L.; Xiong, Z. Use of supplementary cementitious materials in seawater–sea sand concrete: State-of-the-art review. *Constr. Build. Mater.* **2024**, *425*, 136009. [CrossRef]
37. Dobiszewska, M.; Bagcal, O.; Beycioğlu, A.; Goulias, D.; Köksal, F.; Płomiński, B.; Ürünveren, H. Utilization of rock dust as cement replacement in cement composites: An alternative approach to sustainable mortar and concrete productions. *J. Build. Eng.* **2023**, *69*, 106180. [CrossRef]
38. Liu, Y.; Wang, B.; Fan, Y.; Yu, J.; Shi, T.; Zhou, Y.; Song, Y.; Xu, G.; Xiong, C.; Zhou, X. Effects of reactive MgO on durability and microstructure of cement-based materials: Considering carbonation and pH value. *Constr. Build. Mater.* **2024**, *426*, 136216. [CrossRef]
39. Peng, Y.; Liu, Y.; Zhan, B.; Xu, G. Preparation of autoclaved aerated concrete by using graphite tailings as an alternative silica source. *Constr. Build. Mater.* **2021**, *267*, 121792. [CrossRef]
40. Zhang, C.; Li, B.; Yu, Y.; Zhang, Y.; Xu, H.; Wang, W.-X. An Investigation of the Mechanical Properties of Basalt Fibre-Reinforced Graphite Tailings Cement Mortar. *Buildings* **2022**, *12*, 2106. [CrossRef]
41. Zhou, Z.; Xie, N.; Cheng, X.; Feng, L.; Hou, P.; Huang, S.; Zhou, Z. Electrical properties of low dosage carbon nanofiber/cement composite: Percolation behavior and polarization effect. *Cem. Concr. Compos.* **2020**, *109*, 103539. [CrossRef]
42. Shyr, T.-W.; Shie, J.-W. Electromagnetic shielding mechanisms using soft magnetic stainless steel fiber enabled polyester textiles. *J. Magn. Magn. Mater.* **2012**, *324*, 4127–4132. [CrossRef]
43. Baoyi, L.; Yuping, D.; Yuefang, Z.; Shunhua, L. Electromagnetic wave absorption properties of cement-based composites filled with porous materials. *Mater. Des.* **2011**, *32*, 3017–3020. [CrossRef]
44. He, Y.; Lu, L.; Sun, K.; Wang, F.; Hu, S. Electromagnetic wave absorbing cement-based composite using Nano-Fe3O4 magnetic fluid as absorber. *Cem. Concr. Compos.* **2018**, *92*, 1–6. [CrossRef]
45. Xie, S.; Ji, Z.; Li, B.; Zhu, L.; Wang, J. Electromagnetic wave absorption properties of helical carbon fibers and expanded glass beads filled cement-based composites. *Compos. Part A Appl. Sci. Manuf.* **2018**, *114*, 360–367. [CrossRef]
46. Bai, Y.-h.; Zhang, D.-y.; Lu, Y. Foamed concrete composites: Mn–Zn ferrite/carbon fiber synergy enhances electromagnetic wave absorption performance. *Ceram. Int.* **2023**, *49*, 33703–33716. [CrossRef]
47. *JGJ/T 220-2010*; Technical Specification for Plastering Mortar. Standardization Administration of China: Beijing, China, 2010.

48. Jakoby, B.; Beigelbeck, R.; Voglhuber-Brunnmaier, T. Understanding the Shielding Efficiency of a Faraday Grid Cage: A spectral domain approach. *IEEE Antennas Propag. Mag.* **2023**, *65*, 46–56. [CrossRef]
49. Izadifar, M.; Dolado, J.S.; Thissen, P.; Ukrainczyk, N.; Koenders, E.; Ayuela, A. Theoretical Elastic Constants of Tobermorite Enhanced with Reduced Graphene Oxide through Hydroxyl vs Epoxy Functionalization: A First-Principles Study. *J. Phys. Chem. C* **2023**, *127*, 18117–18126. [CrossRef]
50. Chung, D.D.L.; Xi, X. A review of cement-based materials as electroceramics. *Ceram. Int.* **2023**, *49*, 24621–24642. [CrossRef]
51. Li, Y.; Liu, J.; Jin, C.; Lin, H.; Shen, J. Experimental study and mechanism analysis of functional nanocrystalline cellulose to improve the electromagnetic transmission performance of ordinary Portland cement. *Cem. Concr. Compos.* **2023**, *143*, 105272. [CrossRef]
52. Deng, G.; Yang, Y.; Zhou, Q.; Lei, Y.; Yue, L.; Yang, T. Lightweight and broadband electromagnetic wave absorbing foamed cement-based composites incorporated with hybrid dielectric fibers. *Constr. Build. Mater.* **2022**, *327*, 126931. [CrossRef]
53. Bian, P.; Yu, Q.; Zhan, B.; Guo, B.; Gao, P.; Hong, L.; Yang, Y.; Wang, C. Broadband electromagnetic wave absorption cement-based composite using foam-loaded KH550@Fe3O4 nanoparticles. *Constr. Build. Mater.* **2024**, *449*, 138324. [CrossRef]
54. Ma, C.; Xie, S.; Wu, Z.; Ji, Z.; Wang, J. Research and simulation of electromagnetic wave absorbing performance for lightweight cement-based materials containing expanded polystyrene with different particle sizes and carbon black. *Constr. Build. Mater.* **2024**, *430*, 136496. [CrossRef]

Disclaimer/Publisher's Note: The statements, opinions and data contained in all publications are solely those of the individual author(s) and contributor(s) and not of MDPI and/or the editor(s). MDPI and/or the editor(s) disclaim responsibility for any injury to people or property resulting from any ideas, methods, instructions or products referred to in the content.